03

Combined volume discharge radiation in presence of a diffracted shock wave front

© A.A. Ivanova, I.V. Mursenkova

Department of Physics, Moscow State University,
119991 Moscow, Russia
e-mail: iaanniva.phys@gmail.com

Received July 29, 2025
Revised September 29, 2025
Accepted September 29, 2025

Results of an experimental study of a combined nanosecond volume discharge in air in front of a diffracted shock wave with various shock wave front positions in the discharge glow are reported. With Mach numbers of 3.0−4.4, radiation and current of a discharge initiated at pulsed voltage of 25 kV were recorded. It was found that discharge glow duration in the presence of a shock wave was longer than in still air, and time dependence of glow intensity was non-monotonic and had an additional maximum at the afterglow stage. Kinetic processes in a plasma region with a length from 7−40 mm, which interacted with a shock wave at the afterglow stage, were explored.

Keywords: shock wave, combined nanosecond volume discharge, gas-discharge plasma, ICCD camera, plasma radiation.

DOI: 10.61011/TP.2026.02.62875.190-25

Introduction

Interaction between shock waves and gas discharge plasma has been studied over the last decades [1–10]. The investigations are important for solution of high-speed plasma gas dynamics problems. Complexity of general problem solution is in that plasma processes in the time interval $10^{-10}-10^{-7}$ s should be considered together with gas dynamic phenomena, including gas heating, fluid density variation, diffusion and other processes in the range of $10^{-6}-10^{-4}$ s. To date, experimental studies should be continued for deep understanding of the effect of all processes on the interaction between shock waves and plasma.

Features of shock waves in plasma of low-pressure steady-state glow discharges with durations up to several milliseconds was reported in the literature of the late 20th and early 21st centuries [1,2,10,11]. Shock wave intensity attenuation, shock wave front expansion and change in the front shape, and acceleration in plasma region were observed during the experiments [1,11]. Shock wave parameters varied as the shock wave moved through the plasma region, and after leaving the domain, the wave front structure was restored. Detailed measurements were carried out when investigating plane shock wave motion in gas-discharge plasma of steady-state glow discharge in argon and argon/nitrogen mixtures in cylindrical tubes [2]. Numerical calculations have shown that the main contribution to the change in flow structure is made by spatially inhomogeneous heating of neutral plasma component [2]. Temperature and density gradients, shock wave front curvature affect the shock wave motion pattern in the weakly ionized plasma region. Experimental study of the glow-discharge plasma effect on a head shock wave [6] has shown a change in shock wave configuration in a time range of 20−30 μs.

Numerical simulation of flows with shock waves was based on primarily thermal mode of action of steady-state discharges [6,12,13]. Modes of supersonic flow past bodies were explored, flow structure and stability in different geometrical configurations of the energy deposition domain in the incident flow were reviewed [12,13]. Stable modes of flow past body, featuring flow restructuring, formation of detached flow regions, effect of energy deposition heat wake, were detected. Various flow modes were implemented in interaction between shock waves and high-temperature (low density) gas regions. Consequently, shock wave front curvature, generation of supersonic jets and large-scale eddies, instability evolution were observed.

At the same time, non-thermal effects in shock wave motion through the plasma region were observed experimentally. Thus, significant amplification of optical radiation near the shock wave was noted in the glow-discharge plasma at the afterglow stage [10]. Shock wave intensity variation caused a change in the effect. Investigation data analysis implied that energy electrons from the double electric layer region near the shock wave front could additionally contribute to radiation. Later it was shown theoretically [14] that at the shock wave front, jumps in charge density and plasma potential associated with thermal gradients in quasi-steady-state plasma can be observed. The effect of atomic and molecular origin of gases on the shock wave motion pattern in the glow-discharge plasma was determined by means of kinetic calculations [4]. Simulation was performed in argon for in-depth study of electron cooling process behind the shock wave front [14]. The model included the empirical correlation between electron

temperature and electric field strength, and considered high thermal diffusivity of electrons compared with ions. Kinetic simulation was used to calculate the local electron temperature and clarify plasma dynamics near the shock wave. Neither unambiguous correlation between processes in the steady-state discharge plasma and shock wave motion pattern nor inverse effect of the shock wave on plasma condition were detected.

In recent decades, nanosecond discharges with volume and surface geometry have been extensively studied with reference to plasma gas-dynamics problems [1,3,7,8,9,15,16]. Numerous experimental and theoretical studies have shown that perturbations caused in high-velocity gas flows by local changes in flow parameters induced by energy input could effectively influence shock waves, air drag of streamlined surfaces, thermal loads, etc. [3,7,15,17].

Perturbation propagation and generation of shock-wave structures due to pulse energy deposition and fast gas heating determine the mode of nanosecond discharge action on high-velocity flows [5,16,18–21]. At present, experimental and numerical studies are focused on investigating processes taking place in the presence of shock waves in nonsteady-state gas-discharge plasma. The aim of numerous studies is to describe the fast gas heating mechanism in nanosecond discharges induced by reactions involving excited atom and molecule states generated under the action and further relaxation of strong electric fields [3,7,8,15,22]. This is important for application to plasma-assisted combustion and plasma gas-dynamics problems.

The problem of interaction between plane shock waves and combined nanosecond volume discharge plasma was studied experimentally in various settings [16,18–20,23–28]. It was shown that formation of localized plasma region is determined by the strength of reduced electric field in front of the shock wave and, consequently, by significant electron concentration [12,29]. Dynamics of flow after discharge was experimentally studied in air flows with plane shock waves at Mach numbers up to 5 [16,19,20]. Pulse energy deposition at the energy deposition domain boundaries results in discontinuity breakdowns. Evolution and interaction of discontinuities after discharge define the features of generation and motion of shock wave configurations in a time range up to hundreds of microseconds. In real gas flow conditions during movement of shock waves with curved fronts, the flow structure becomes complicated due to the interaction of various flow components.

Gas dynamic simulation of flow with a plane shock wave [16,30] considered the discharge domain as a source of energy immediately embedded in the flow and translated into internal gas energy. Mathematical model used a system of two-dimensional non-steady-state Navier–Stokes equations with boundary conditions corresponding to experimental ones [30,31]. By comparing the simulation data and experimental images, interaction between the plane shock wave and energy deposition domain was analyzed and flow dynamics was studied. As a result of experimental data generalization and numerical simulation, the amount of released heat energy was determined in different initial conditions. Later numerical calculations showed that energy deposition time could affect the flow pattern [20,23,24,32], therefore processes in the nanosecond discharge plasma should be analyzed in a wide time range.

Experiments explored current and radiative properties of a volume discharge in the presence of a plane shock wave front and in still air [5,9,32]. Correlation between glow pulsations near the front and current oscillations was shown [9,23]. Glow duration in the experiments depended on the plane shock wave position in the discharge volume at the voltage application time. Long-lasting afterglow was observed near the shock wave front. This is indicative of reactions, which can affect the gas dynamic flow.

Despite the versatile theoretical and experimental studies of interaction between shock waves and plasma, it is still important to continue investigating plasma processes in conditions of high-velocity gas dynamic flow with shock waves of different geometries. The aim of this study was to investigate spatial distribution and radiation dynamics of the combined nanosecond volume discharge interacting with the diffracted shock wave front in a rectangular channel. Focus was made on investigating the effect of shock wave front geometry on radiation dynamics, and also on time dependences of glow on plasma parameters.

1. Experimental Setup and Measurement Technique

Experimental setup consisted of a diaphragm type shock tube with a low pressure chamber, 297 cm in length, with 48×24 mm rectangular cross-section. Air with initial pressure of $p_0 = 10-100$ Torr was used as the driven gas, and helium at pressure up to 10 atm was used as the driver gas. Rupture of the diaphragm led to generation of a plane shock wave, behind which the homogeneous cocurrent flow was established. Supersonic cocurrent flow time was $300-600\,\mu$s at the Mach numbers of shock waves $M = 3.0-4.4$. Shock wave front velocities were measured using piezoelectric pressure sensors installed along the channel (the measurement accuracy up to 0.1 m/s).

A test section (Figure 1), whose dimensions were equal to the shock tube channel cross-section, was placed at the end of the low-pressure chamber of the shock tube. Side walls of the section were made of plane-parallel quartz plates. Flow in the test sections was close to two-dimensional, which was demonstrated experimentally and supported by numerical calculations [24]. A $6 \times 2 \times 48$ mm $(x \times y \times z)$ parallelepiped-shaped obstacle (Figure 1, *b*) was placed on the test section bottom wall to produce complex gas dynamic flow with a diffracted shock wave and inhomogeneous flow behind its front.

Shock wave front in the straight channel of the shock tube is a plane separating low pressure and high pressure areas. As the plane shock wave passed the obstacle, it diffracted in

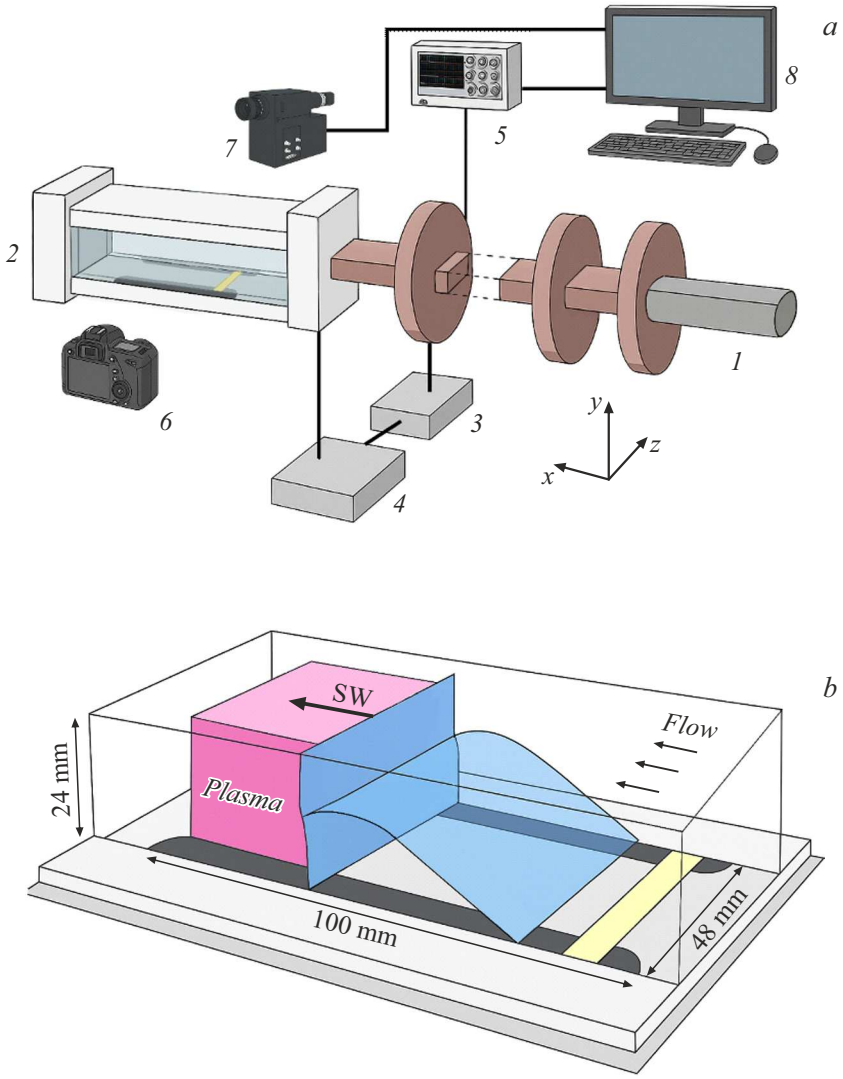

Figure 1. *a* — experimental setup: *1* — shock tube, *2* — test section, *3* — process synchronization unit, *4* — discharge starting unit, *5* — oscilloscope, *6* — photo camera, *7* — ICCD camera, *8* — data storage and processing unit; *b* — diagram of flow in the test section with diffracted shock wave.

such a way that its front took a curved shape [24,32]. In a homogenous fluid, as the shock wave moves away from the obstacle, the curvature of its front decreases (Figure 2, $a-c$), as shown in [32], and the shock wave almost regains its plane shape at $x > -10$ mm.

Copper surface discharge electrodes 0.1 mm in thickness were placed on the top and bottom dielectric walls of the test section spaced at 24 mm (Figure 1, 3, a). When investigating the shock wave front motion in the test section, the end of electrodes was taken as the zero x coordinate. Circuit diagram of the combined nanosecond volume discharge, consisting of two surface creeping discharges, is shown in Figure 3, a. When pulse voltage was applied, upper and lower plasma electrodes with an area of 30×100 mm were formed on the dielectric surfaces to provide volume preionization by means of ultraviolet light [25,26]. Volume gas breakdown occurred at time of pulsed discharge of a capacitor charged to the working voltage $U = 25$ kV (Figure 3, a). Maximum electric energy accumulated in the main capacitor was 0.72 J. Total current flowing in the combined volume discharge circuit was recorded by a tailor-made low-inductance shunt installed in the grounding electrode circuit. Current waveforms were recorded using the Tektronics TPS 2014 four-channel digital storage oscilloscope. Figure 2, b shows a current oscillogram recorded during discharge initiation in stationary homogeneous medium showing typical discharge current oscillations. Mean discharge current time was about 600 ns. Discharge initiation was synchronized with piezoelectric pressure sensor signals in the shock tube channel and was performed by a pulse applied from a generator to a controlled gap (Figure 3, a). Such setup provided discharge initiation with a pre-defined shock wave front position; length of the generated plasma region was $7-40$ mm.

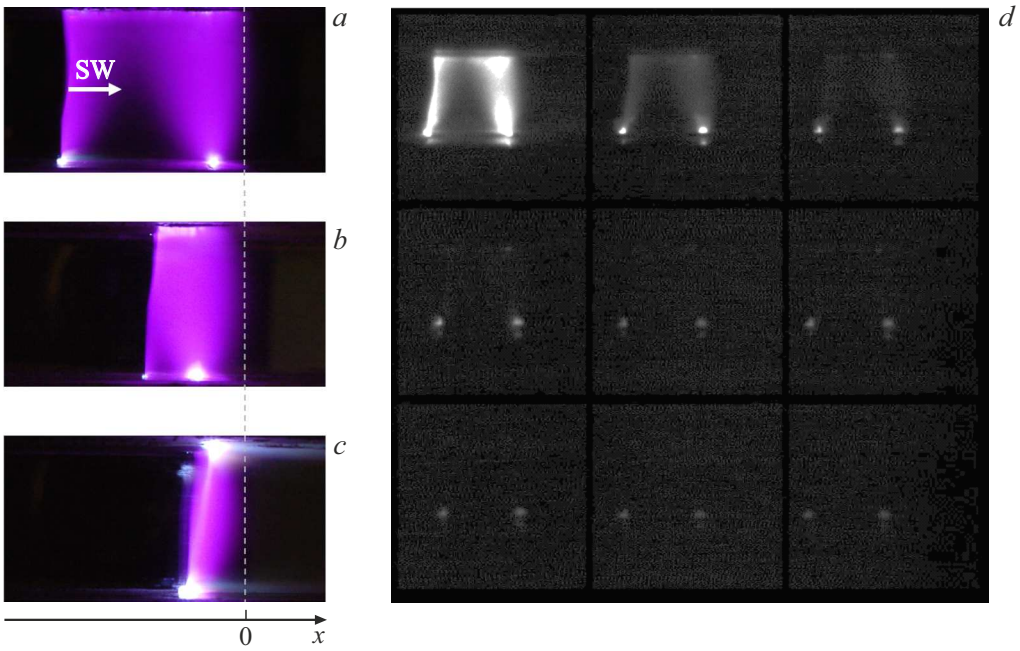

Figure 2. Photographs of discharge glow in front of the diffracted shock wave at $x = -27$ (a), -11 (b), -5 mm (c) and 9-frame image (d) corresponding to (a) (exposure/pause — 100/100 ns). $M = (4.2 \pm 0.1)$, $p_0 = 9$ Torr.

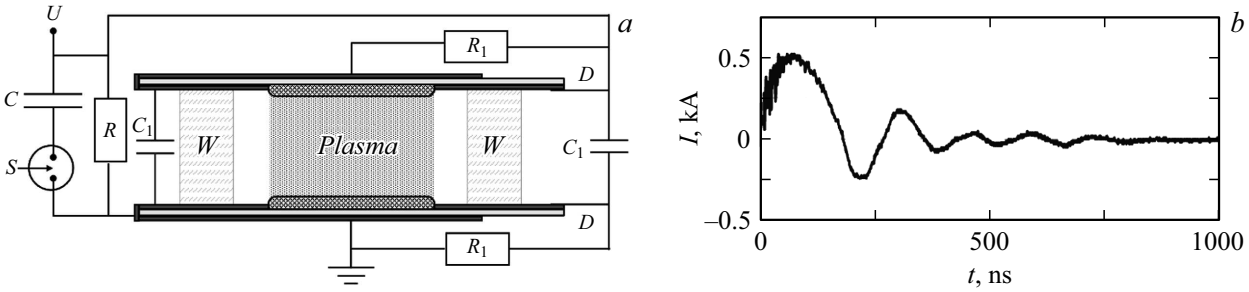

Figure 3. a — discharge circuit diagram: $C = 2300$ pF, $C_1 = 470$ pF, $R = 1$ kW, $R_1 = 1.5$ kW, $U = 25$ kV; S — controlled gap, W — quartz walls of the test section, D — dielectric wall; b — current waveform in still air at 23 Torr.

Combined volume discharge radiation in still air and in flows with shock waves was recorded through transparent walls of the test section. Photo cameras installed on both sides of the test section were used for recording, and time integral glow was recorded with exposure corresponding to discharge glow time. Photographs were also used to accurately identify the shock wave front position in the plasma region when pulse voltage was applied. Shock wave front shift during exposure was max. 1 mm. Photographs were processed using a graphics editor for sharpening. K011 nanosecond-resolution ICCD camera was used in a nine-frame recording mode with an exposure of 100 ns and frame intervals from 100 ns to 300 ns [27]. Spectral sensitivity of the camera was 380–880 nm, active photocathode area was 13×17.3 mm. ICCD images were processed using built-in software and proprietary software code developed by the authors.

To obtain time dependences of discharge glow intensity, scanning of volume discharge glow in the central part of the channel and of surface regions near the channel walls was performed. First, brightness integration (summation of the number of bright pixels) was performed using a band with a fixed width. The obtained values were normalized to the plasma region length the shock wave front, allowing to consider differences in glow region dimensions in various experiments. Thus, the obtained values were proportional to the radiation intensity from unit volume. Then, the intensities were additionally normalized to the maximum value. Such technique was used to obtain time dependences of plasma radiation intensity in the volume and surface discharge radiation domains and trace plasma region radiation dynamics during interaction with the shock wave.

Image processing error was defined by statistical brightness fluctuations, scanning region selection uncertainty and errors of normalizing to the plasma region dimensions. Statistical brightness error was determined by dark frames obtained without discharge by calculating the standard deviation of intensity in the scanning region. Systematic

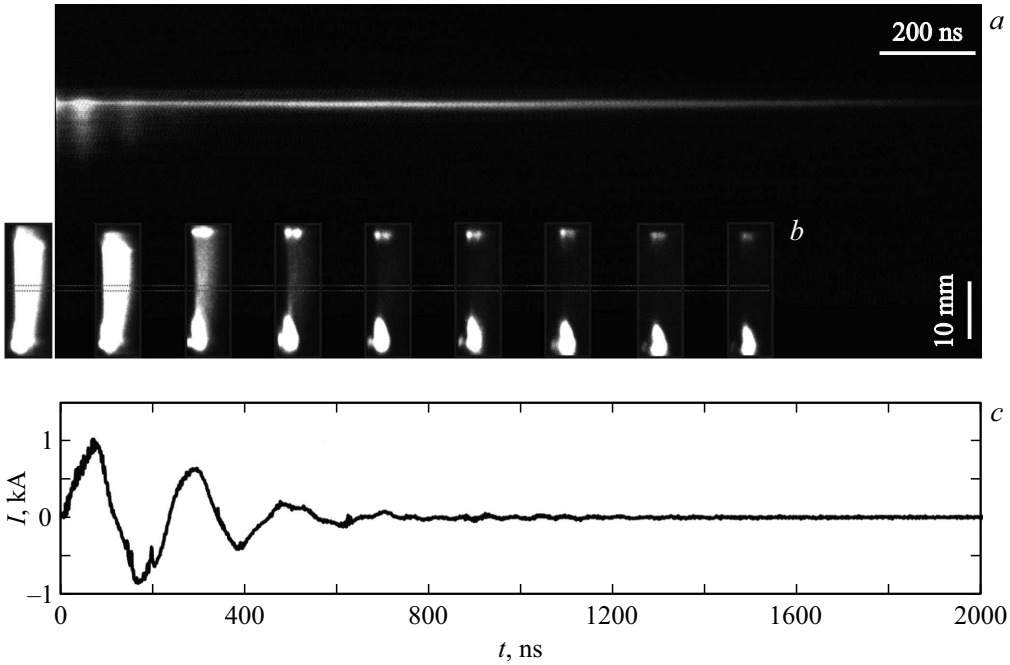

Figure 4. Time streak (a) and ICCD nine-frame image (b) (exposure/pause — 100/100 ns) of volume discharge glow in front of the plane shock wave; c — current waveform. $M = 4.60$, $p_0 = 6$ Torr, $x = -14$ mm.

error associated with selection of the integration domain was estimated by varying the scanning line position and width within 5 px; spread of the obtained values was considered in the total error. Error associated with normalization to the plasma region length and maximum intensity coordinate was considered separately: variations of these parameters within the image resolution were 1 px.

2. Experiments for investigation of interaction between a shock wave and plasma region

Experiments simultaneously analyzed discharge time characteristics and plasma glow behavior at various Mach numbers, initial pressures and plasma region lengths. Time characteristics of discharge were determined from the analysis of nanosecond-resolution ICCD images and current waveforms. Spatial characteristics of gas dynamic flow in the channel were determined earlier by analyzing high-speed schlieren photographs and discharge glow photographs [24,32]. Various diagnostics techniques were used for in-depth study of interaction processes between the shock wave and plasma.

Figure 2, $a-c$ shows discharge glow in front of the diffracted shock wave front with different front positions corresponding to different plasma region lengths. Volumetric nature of pulse breakdown is traced by spatial glow distribution in photo images visualizing the discharge current passage region. All images clearly show the left boundary of glow, visualizing the diffracted shock wave front, and the right boundary corresponding to the plasma volume edge. When the shock wave front is in the discharge volume at the pulse voltage application time, electric field strength assigned to the concentration of neutral molecules appears to be higher before the front. This leads to the growth of electron concentration in the low pressure region due to higher ionization coefficient [29] and is followed by volume current and glow localized in front of the shock wave front [18,19,32].

Figure 2, d shows nine ICCD discharge images demonstrating different glow stages. The first two images show the volume glow phase lasting 100−200 ns, which corresponds to the current in a domain limited by the diffracted shock wave front. The next images show gradual decay of the volume discharge phase, total length of which exceeds 500 ns. Then long-lasting afterglow of surface discharges on the top and bottom walls of the chamber takes place until 2000 ns.

Figure 4 shows time streak of glow in the central region of the channel (Figure 4, a), series of ICCD images (Figure 4, b) and discharge current waveform (Figure 4, c) during interaction between the discharge and plane shock wave. Radiation from the plasma region persists longer than 1000 ns after termination of discharge current, which reflects complex relaxation dynamics in the domain in front of the shock wave front as noted in [23,28]. Surface discharge glow time can also exceed 1500 ns. The glow scan was obtained from the center of the channel shown with dashed line in Figure 4, b.

Then, time profiles of plasma afterglow intensity in volume and surface discharge domains were compared at

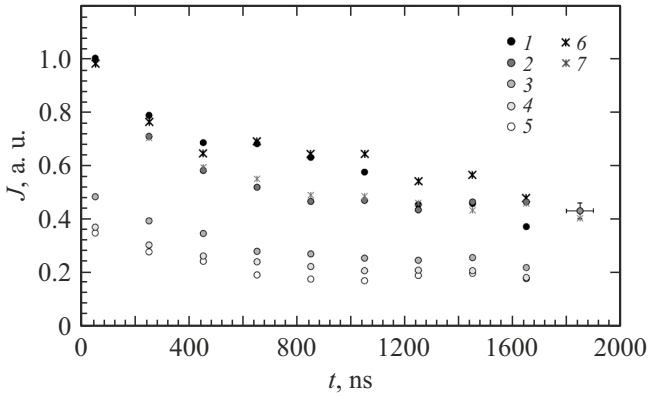

Figure 5. Time dependence of discharge glow intensity in the center of the channel (*1*–*5*) and upper near-surface region (*6*, *7*) at the plasma region length of 7 (*1*, *6*), 11 (*2*, *7*), 16 (*3*), 20 (*4*), 22 mm (*5*). $M = (4.2 \pm 0.1)$, $p_0 = 9$ Torr.

different lengths of plasma region in front of the shock wave front (Figure 5). Non-monotonic decrease of glow intensity is observed in all above-mentioned cases. Maximum intensity corresponds to the discharge current stage (up to 500 ns) followed by exponential decay. However, in the range of 650–1450 ns, there is a repeated increase in intensity, whose magnitude and time depend on the shock wave position at the discharge initiation time, i.e. on the plasma region length and, consequently, on plasma parameters before the front. Thus, with the shortest plasma region length (7 mm), intensity starts increasing after 450 ns, reaches its maximum at 650 ns and decays again. When the plasma region length is 11 mm, radiation starts increasing after 950 ns with its maximum at 1150 ns followed by decay. For longer plasma regions (16–22 mm), intensity starts increasing even later and reaches its maximum at 1450 ns. The same dependence pattern is also retained at other Mach numbers of shock waves: intensity decay observed until 1050–1250 ns is followed by growth and reaching the second maximum in the area of 1450 ns.

Intensity increase was estimated quantitatively with respect to the values on the exponential decay curve. Thus determined maximum exceedance of intensity was 25 % at $x = -7$ mm, 21 % at $x = -11$ mm, 14 % at $x = -16$ mm with processing error of 3 %. At higher plasma region lengths, intensity increase is less pronounced and can be within the processing error (Figure 5, rows 4, 5). Thus, the presence of repeated increase in glow intensity after termination of discharge current may be considered to be valid and can be associated with kinetic processes defined by plasma state in front of the shock wave.

The same time dependence of glow intensity is also observed in the time range up to 2500 ns (Figure 6). After termination of discharge current, there is an exponential intensity decay up to 1050–1250 ns followed by repeated increase with its maximum at 1450 ns and then by an exponential decay after 1800 ns. Thus, the typical radiation evolution is retained: maximum intensity during current, decay, secondary growth and subsequent decay.

Obtained dependences correspond to the results of previous studies of interaction between the plane shock wave and volume discharge plasma, where similar patterns were noted. Time dynamics of volume glow of plasma region in front of the plane shock wave was studied on the basis of streak images (Figure 4, *a*, 6, *b*). Thus obtained dependences were compared with ICCD results for more detailed study of glow decay pattern of the plasma region in front of the shock wave. Analysis of volume discharge glow scan in front of the plane shock wave (Figure 6, *b*) has shown that repeated glow intensity increase is observed in the range from 700 ns to 1000 ns, which corresponds to results for the diffracted shock wave.

Figure 7 shows dependence of the intensity increase time at the discharge afterglow stage t^* on the plasma region length for two types of shock waves: diffracted *1* and plane *2*. This time corresponds to the radiation increase time after termination of discharge current. The dependence shows that at long plasma region lengths (more than 15 mm), this time reaches 1000 ns, while at short lengths (less than 15 mm), it is about 150–550 ns on average.

3. Analysis of relaxation processes in plasma in front of the shock wave front

At high electric field strengths, a considerable part of discharge electric energy in air is spent for molecule ionization, excitation of vibrations and electronic degrees of freedom of nitrogen and oxygen molecules [7,15,29]. Typical relaxation process times were estimated in the nanosecond discharge plasma. Mean concentration of electrons in the discharge plasma region was estimated on the basis of relation with the discharge current maximum [9]:

$$j_{\max} = I_{\max}/S = e \cdot n_e \cdot V_d(E/N), \qquad (1)$$

where $j_{\max}$ is the current density, e is the electron charge, n_e is the electron concentration, S is the current cross-section, $V_d(E/N)$ is the electron drift velocity in an electric field with a strength E with neutral particle concentration N. Maximum discharge current $I_{\max}$ in experiments depended on the initial pressure and shock wave position at voltage application time and was equal to 600–1000 A. Reduced electric field strength estimated by the electric circuit parameters (Figure 3, *a*) was $E/N = (3-15) \cdot 10^{-15}$ V $\cdot$ cm^2 = (300–1500) Td. Electron drift velocity V_d in the implemented range of E/N was 10^7–10^8 cm/s [33]. Thus calculated electron concentration in the domain in front of the shock wave front and in the near-surface regions was within $(5-10) \cdot 10^{13}$ cm^{-3} and $(1-5) \cdot 10^{14}$ cm^{-3}, respectively. In still air, electron concentration in the domain was $\sim 10^{12}$ cm^{-3}. Electron and ion recombination time in the volume discharge plasma

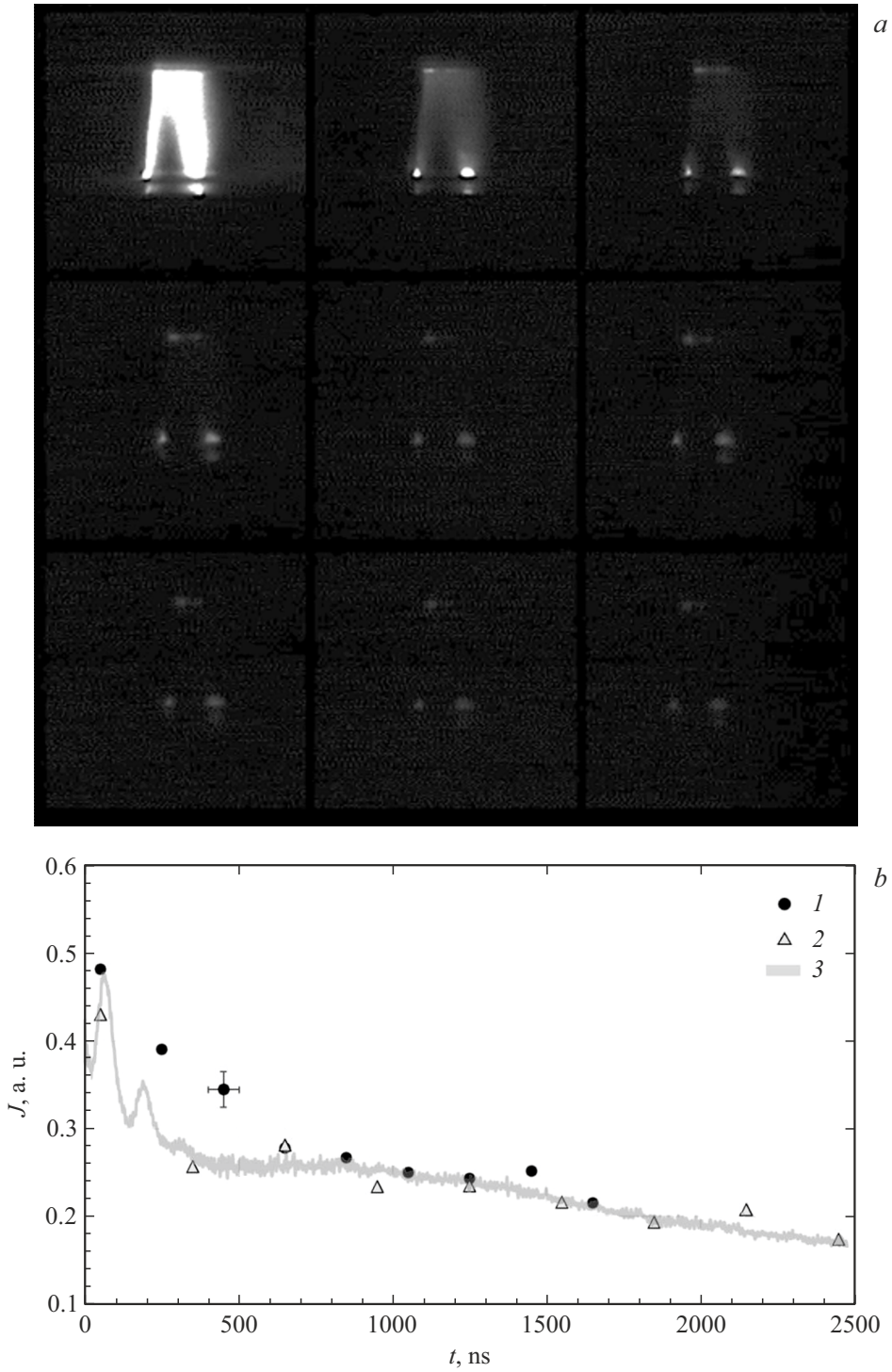

Figure 6. *a* — Nine-frame image of discharge glow with shock wave at $x = -16$ mm (exposure/pause — 100/100 ns), *b* — time dependences of glow intensity in the center of domain at $x = -16$ mm (*1*, exposure/pause — 100/100 ns), $x = -17.5$ mm (*2*, exposure/pause — 100/200 ns), $x = -14$ mm (*3*, from glow scan in Figure 4, *a*). $M = (4.2 \pm 0.1)$, $p_0 = 9$ Torr.

was about 300 ns, and in the surface discharge plasma was 50 ns. During air plasma disintegration, a part of energy released during electron and ion recombination is converted into heat [7,15].

To describe plasma glow dynamics in front of the plane shock wave front, correlation with gas dynamic perturbations was considered [23]. When pulse discharge was initiated, discontinuity breakdown at the shock wave front occurred [5,20], and one of the generated shock waves continued moving through the plasma region, compressing it. Since the emission is defined by the second positive nitrogen system bands [9,23], radiation intensity is propor-

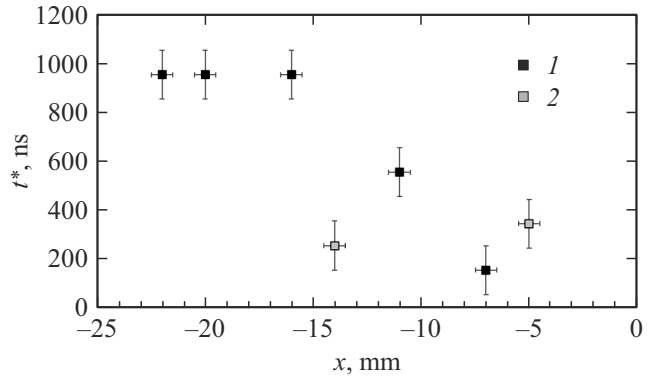

Figure 7. Dependence of the discharge afterglow intensity increase time on the plasma region length (*1* — diffracted SW, *2* — plane SW).

tional to the concentration of nitrogen molecules in the excited state $C^3\Pi_u$ [29]. Calculations of the discharge glow dynamics with the plane shock wave implied that the state $C^3\Pi_u$ is populated through collisional reactions of nitrogen molecules in the metastable state $A^3\Sigma_u^+$, concentration of which increased as the shock wave passed through the plasma region [23,33,34]. The calculated dependence has shown good agreement with the radiation dynamics where glow intensity increase was observed during 200 ns after termination of discharge current, and then there was intensity decay with typical time of about 600 ns [23,33]. Without considering the compression of plasma region by the shock wave, monotonic radiation decay was observed at the afterglow stage. Calculations for the experiments with the diffracted shock wave showed a similar discharge afterglow dynamics despite a more complex flow structure, which confirms that kinetic processes in the plasma region before front are similar. As the plasma region length decreases, i.e. electron concentration increases, afterglow dynamics becomes more pronounced (Figure 5). As the Mach number grows, a more rapid intensity increase is observed at the afterglow stage.

Energy of electronic degrees of freedom of molecules (ET relaxation) can change into kinetic energy leading to gas heating [3,7,15,22]. At the afterglow stage, these are processes involving molecules in metastable states [15,35], typical times of which depend on the concentrations of excited molecules. Population of metastable states of molecular nitrogen $A^3\Sigma_u^+$ and $B^3\Pi_g$ (with lifetimes 13 s and 6.5 μs, respectively) in air at low pressures remains high during several microseconds after termination of discharge current [15,22] and can also affect the perturbation motion.

Conclusion

This study has experimentally investigated the interaction of combined nanosecond volume discharge with diffracted shock wave in air. Photographic and ICCD recording of discharge glow was used to detect non-monotonic plasma glow decay after termination of discharge current in interaction with diffracted shock wave. It has been found that afterglow intensity had an additional maximum in the range from 500 ns to 2000 ns, which depended on the plasma region length in front of the shock wave front. Repeated glow increase effect is most pronounced at the minimum plasma region length in front of the shock wave front, and as the minimum plasma region length grows the increase is less pronounced and occurs later. Comparison with the results of studies of plane shock waves has shown that the shock wave front shape (plane or curved) had no significant effect on the glow behavior. Thus, the repeated emission increase effect indicates a connection between the gas-dynamic influence of the shock wave and the radiation process.

Electron excitation relaxation and vibrational-translational relaxation processes, whose typical times are in the range up to several microseconds, are the governing processes in the afterglow dynamics. Collisional processes of metastable nitrogen molecules with transition to the emitting state $C^3\Pi_u$ are the key processes. At electron concentrations typical of the volume discharge plasma, population of this state is performed both by direct electron impact and by nitrogen molecule collisions in metastable states. This considerably changes the emission kinetics in the presence of a moving shock wave front compared with the radiative decay in still air. Thus, within a time range up to 2 μs, effects associated with transitions of metastable molecules to radiative states form the observed afterglow dynamics. The involved reactions can in turn affect the supersonic flow characteristics. Thus, the relaxation processes in the nanosecond discharge plasma play a decisive role in the radiation dynamics during interaction with shock waves. Results of the study are focused on clarification of the mechanism of interaction between shock waves and plasma inhomogeneities. They may be used for optimization of systems of plasma control of shock-wave configurations in high-speed flows, including aircraft air intake ducts.

Funding

A.Ivanova's work was supported by the Theoretical Physics and Mathematics Advancement Foundation „BASIS“, grant 24-2-10-54-1.

Conflict of interest

The authors declare no conflict of interest.

References

[1] V. Fomin, P. Tretyakov, J.-P. Taran. Aerospace Sci. Technol., **8** (5), 411 (2004). https://doi.org/10.1016/j.ast.2004.01.005
[2] S.O. Macheret, Yu.Z. Ionikh, N.V. Chernysheva, A.P. Yalin, L. Martinelli, R.B. Miles. Phys. Fluids, **13** (9), 13 (2001).
[3] D.A. Xu, M.N. Shneider, D.A. Lacoste, C.O. Laux. J. Phys. D: Appl. Phys., **47** (23), 235202 (2014). DOI: 10.1088/0022-3727/47/23/235202

[4] G. Cicala, D. Bruno, M. Capitelli, S. Longo, A.C. Rainò. J. Physics D: Appl. Phys., **57**, 375 (2010). DOI: https://doi.org/10.1140/epjd/e2010-00066-y
[5] I. Doroshchenko, I. Znamenskaya, A. Kuznetsov, I. Mursenkova, N. Sysoev. Tech. Phys., **63** (5), 662 (2018). DOI: 10.1134/S1063784218050067
[6] T.A. Lapushkina, A.V. Erofeev, O.A. Azarova, O.V. Kravchenko. Tech. Phys., **64** (1), 34 (2019). DOI: 10.1134/S1063784219010201
[7] A.Yu. Starikovskiy, N.L. Aleksandrov. Plasma Phys. Rep., **47** (2), 148 (2021).
[8] D. Knight, N. Kianvashrad. Energies, **15**, 9645 (2022).
[9] N. Arkhipov, I. Znamenskaya, I. Mursenkova, I. Ostapenko, N. Sysoev. Moscow Univ. Phys. Bull., **69**, 96 (2014).
[10] N. Siefert, B.N. Ganguly, P. Bletzinger. Phys. Rev. E, **72**, 066402 (2005).
[11] A.I. Klimov, A.N. Koblov, G.I. Mishin, Yu.L.Serov, I.P. Yavor. Sov. Tech. Phys. Lett., **8**, 240 (1982).
[12] P.Yu. Georgievskii, V.A. Levin. Fluid Dyn., **38**, 794 (2003). DOI: 10.1023/B:FLUI.0000007841. 91654.10
[13] P.Yu. Georgievskiy, V.A. Levin, O.G. Sutyrin. Tech. Phys. Lett., **44**, 10 (2018).
[14] A.K. Sukhov. Moscow Univ. Phys. Bull., **76**, 47 (2021). DOI: 10.3103/S0027134921010100
[15] S. Nagaraja, V. Yang, I. Adamovich. J. Phys. D: Appl. Phys., **46**, 155205 (2013).
[16] I. Znamenskaya, I. Mursenkova, I. Doroshchenko, I. Ivanov. Phys. Fluids, **31** (11), 116101 (2019).
[17] X.G. Ma, J. Fan, Y.K. Wu, X.W. Liu, R. Xue. Phys. Fluids, **34** (8), 086102 (2023).
[18] I.A. Znamenskaya, A.E. Lutsky. *Issledovanie evolyutsii i vzaimodeistviya razryvov techeniya v kanale pod deistviem impulsnogo vlozheniya energii* (Preprint IPM im. M.V. Keldysha RAN, 2005), № 88. (in Russian)
[19] I.A. Znamenskaya, D.A. Koroteev, D.M. Orlov, I.V. Mursenkova, A.E. Lutsky, I.E. Ivanov. *Shock wave interaction with nanosecond transversal discharges in shock tube channel* (ISSW-26. Book of Abstracts. 2007), p. 1–7.
[20] I. Znamenskaya, A. Kuznetsov, I. Mursenkova, I. Doroschenko. J. Phys.: Conf. Series, **1112**, 012006 (2018).
[21] S.B. Leonov, V. Petrishchev, I.V. Adamovich. J. Phys. D: Appl. Phys., **47**, 465201 (2014).
[22] N. Aleksandrov, E. Anokhin, S. Kindysheva, A. Kirpichnikov, I. Kosarev, M. Nudnova, S. Starikovskaia, A. Starikovskii. J. Phys. D-Appl. Phys., **45**, 255202 (2012). DOI: 10.1088/0022-3727/45/25/255202
[23] A. Kuznetsov, I. Mursenkova, P. Ulanov. Tech. Phys. Lett., **45** (12), 1266 (2019). DOI: 10.1134/S1063785019120228
[24] A.Yu. Kuznetsov, I.V. Mursenkova. Appl. Phys., **5**, 16 (2016).
[25] H. Brunet, P. Vincent. J. Appl. Phys., **50** (7), 4708 (1979). DOI: 10.1063/1.326527
[26] V.M. Borisov, A.I. Demin, A.V. Eltsov, V.P. Novikov, O.B. Khristoforov. Kvantovaya elektronika, **26** (3), 204 (1999) (in Russian).
[27] Electronic resource. Available at: https://www.vniiofi.ru/depart/r5/k011.html?ysclid=m471hwzuxa251158883
[28] A.Yu. Kuznetsov, I.V. Mursenkova. Appl. Phys., **5**, 16 (2016).
[29] Yu.P. Raizer. *Gas Discharge Physics* (Springer, Berlin, 1991)
[30] I. Ivanov, I. Kryukov, D. Orlov, I. Znamenskaya. Experiments in Fluids, **48** (4), 607 (2010).
[31] G. Glushko, I. Ivanov, I. Kryukov. Math. Models Comput. Simul., **2**, 407 (2010).
[32] A. Ivanova, I. Mursenkova. Moscow Univ. Phys. Bull., **78**, 204 (2023).
[33] H. Brunet, P. Vincent. J. Appl. Phys., **50** (7), 4708 (1979). DOI: 10.1063/1.326527
[34] Y. Lebedev, V. Shakhatov. Plasma Phys. Reports, **32**, 568 (2006). DOI: 10.1134/S1063780X06010065
[35] W. Yang, Q. Zhou, S. Qiang, Z. Dong, E. Yan. AIP Advances, **10**, 105311 (2020). DOI: 10.1063/5.0021993

Translated by E.Ilyinskaya